Forced Convection Heat Transfer from a Sphere to Non-Newtonian Power Law Fluids

S. D. Dhole and R. P. Chhabra
Dept. of Chemical Engineering, Indian Institute of Technology, Kanpur, 208 016, India

V. Eswaran
Dept. of Mechanical Engineering, Indian Institute of Technology, Kanpur, 208 016, India

DOI 10.1002/aic.10983
Published online September 8, 2006 in Wiley InterScience (www.interscience.wiley.com).

The effects of Reynolds number (Re), Prandtl number (Pr), and power law index (n) on the heat-transfer characteristics of an unconfined sphere submerged in an isothermal and incompressible power law fluid, for different thermal boundary conditions (isothermal and isoflux) on the sphere surface, have been investigated numerically for the 2-D axisymmetric and steady flow by using a finite volume method over the ranges of conditions as $5 \leq Re \leq 200$, $1 \leq Pr \leq 400$ *(the maximum value of the Peclet number is 2000), and* $0.5 \leq n \leq 2$. *Based on the numerical results obtained herein, simple heat-transfer correlations are developed for the constant-temperature and the constant heat-flux boundary conditions to estimate the value of the Nusselt (Nu) number in a new application. Furthermore, the variation of the local Nu over the surface of the sphere has been studied to delineate the effects of Re, Pr, and n on heat transfer from a sphere, thereby showing the extent of heat transfer from the front and the rear parts of the sphere.* © 2006 American Institute of Chemical Engineers *AIChE J,* 52: 3658–3667, 2006
Keywords: Reynolds number, Prandtl number, power law index, Nusselt number, sphere

Introduction

The flow of fluids and heat/mass transfer from a sphere submerged in fluids represents an idealization of many industrially important processes. Typical examples include such setups as fixed and fluidized bed reactors and slurry reactors. In addition to its practical significance, such elementary flows are also of fundamental significance in their own right. Although it is readily conceded that one frequently encounters ensembles of particles in fixed and fluidized bed reactors, aseptic processing of food particles in tubes, and so forth, experience has shown that a rational understanding of transport phenomena (heat/mass transfer) from an isolated sphere is germane to the successful modeling of multiparticle systems. Consequently, considerable research effort has been expended in studying the rate of heat transfer from a sphere immersed in moving fluids. Over the years, voluminous literature has accrued encompassing various aspects of this model flow including the prediction of Nusselt number for free convection, forced convection, and mixed convection regimes for confined and unconfined spheres. Indeed, based on a combination of analytical and/or numerical and experimental results, it is now possible to predict the value of the Nusselt number for heat and mass transfer from a sphere to Newtonian fluids over wide ranges of conditions (for example, see excellent reviews and books on this subject[1-3]).

In contrast, much less is known about the analogous situation involving the flow of non-Newtonian fluids encountered extensively in chemical, food, and polymer process engineering applications.[4] Little information is available on the prediction of the Nusselt number for a sphere immersed in non-Newtonian fluids, albeit extensive literature is now available on the hydrodynamics of spheres in power law fluids (for example, see Chhabra,[5] Renaud et al.,[6] and Dhole et al.[7]). This work

Correspondence for this article should be addressed to R. P. Chhabra at chhabra@iitk.ac.in.

is thus concerned with the prediction of heat transfer from a sphere immersed in streaming power law fluids.

Previous Work

An inspection of the literature available in this field shows that one can discern two distinct approaches to study the rates of heat (or mass) transfer from a sphere to non-Newtonian fluids. In the first category are the analyses based on the application of the boundary layer flow approximation, where most studies also use the simple power law model to mimic shear-thinning behavior; and the assumption of high Prandtl number is also implicit in most of these studies. Acrivos et al.,[8] Bizzell and Slattery,[9] and Lin and Chern[10] numerically solved the boundary layer flow equations over a sphere by using different solution procedures for the flow and temperature fields and obtained the values of the skin friction and the local Nusselt (Nu) number as functions of the Reynolds (Re) and/or Prandtl (Pr) numbers. On the other hand, in a series of articles, Nakayama and coworkers[11-14] developed a general integral method for analyzing the forced thermal convection in laminar boundary layers from axisymmetric surfaces to power law fluids. Kim et al.[15] solved the same equations using a series expansion technique. These boundary layer solutions give local heat-transfer rates only on the leading edge of the sphere and therefore are of limited utility.

The second category includes the results based on the solutions of the full governing equations such as the approximate solution reported by Kawase and Ulbrecht.[16] They obtained an approximate solution for convective heat/mass transfer from a sphere to power law fluids in the creeping flow regime. Similarly, Westerberg and Finlayson[17] obtained a numerical solution to the momentum and energy equations for the low Reynolds number flow of a generalized non-Newtonian fluid embracing shear-dependent viscosity and viscoelastic effects past spheres. These authors reported both the local and the surface-averaged values of the Nusselt number using temperature-independent physical and thermal properties of Nylon-6 melt. The factors, in decreasing order of effect, influencing the value of the Nusselt number according to their study are the Peclet number, viscous dissipation, shear-thinning, temperature-dependent viscosity, fluid elasticity, and temperature-dependent thermal conductivity. The observation that the fluid viscoelasticity has a slight influence on the value of the Nusselt number is also consistent with the other heat transfer[18] and mass transfer[19] studies for spheres in viscoelastic liquids.

Beyond the creeping flow regime, little is known about the interphase heat and mass transfer between a sphere and non-Newtonian fluids in the forced convection regime. The complications arising from the wake formation around bluff bodies at high Reynolds numbers prevent the possibility of analytical treatments. Using the penetration model, Kawase and Ulbrecht[20,21] developed a general framework to estimate the rate of heat/mass transfer in fluid/particle systems under a range of conditions including those from spheres placed in streaming power law fluids, suspended in stirred vessels, in fixed and fluidized beds, and so forth, simply by choosing an appropriate characteristic velocity and a linear dimension. A few experimental studies are also available in which the rates of heat or mass transfer were measured from single spheres submerged in power law fluids.[22,23] Thus, for instance, Kumar et al.[24] reported the average values of Sherwood number for benzoic acid spheres placed in flowing aqueous carboxymethyl cellulose solutions ($n = 0.85$ and $n = 0.77$). Ogawa et al.[25] carried out an experimental study to determine the effects of viscoelasticity on forced convection mass transfer around a sphere and a cylinder for Reynolds number ranging from 1 to 200. Similarly, Hyde and Donatelli[26] experimentally studied the mass transfer from benzoic acid spheres to power law fluids in the creeping flow regime. In the studies of Kumar et al.[24] and Ogawa et al.,[25] empirical correlations were reported, but none of these has been validated using independent data.

From the above discussion, it is clear that only limited information is available on the forced convection heat transfer from non-Newtonian fluids to spheres outside the creeping flow regime, although no prior results are available for shear-thickening fluids. The values of Prandtl number up to 100–200 are frequently encountered in chemical, petroleum, food, polymer, and oil industries. Furthermore, because of the generally high viscosity of such process streams, the Reynolds numbers often are not excessively high. Therefore, in view of the fact[27] that the flow past a sphere transits to the unsteady and axisymmetric regime in Newtonian fluids at about $\mathrm{Re} = 300$, the assumption of steady and axisymmetric flow in the present study is justified under these conditions. Thus, the objective of this work is to provide extensive numerical results on the forced convection heat transfer from a sphere to power law fluids for sphere Re numbers ranging from 5 to 200, Pr numbers ranging from 1 to 400 (maximum value of Peclet number is 2000), and power law index (n) varying from 0.5 to 2. Numerical values of the Nu number have been obtained for the two commonly used thermal boundary conditions imposed on the sphere surface, that is, constant wall temperature and uniform heat flux. Further insights into heat-transfer phenomena are sought by studying the variation of the local Nu number on the surface of the sphere for a range of Re number, Pr number, and n values. The article is concluded by presenting preliminary comparisons with the scant experimental heat/mass transfer data available in the literature.

Problem Statement and Mathematical Formulation

The two-dimensional (2-D) axisymmetric steady flow of an incompressible and isothermal fluid with a uniform velocity U_∞ and temperature T_∞ over a sphere of diameter D placed in an infinite medium is simulated by considering the flow in an artificial tubular domain with a sphere placed symmetrically on the tube axis with slip boundary conditions prescribed on the tube walls, as described elsewhere[28] and shown in Figure 1. In practice, the boundary condition on the surface of a sphere can be complex, although it is customary to prescribe either a constant temperature T_w (CWT) or an uniform heat flux q_w (UHF) in analytical or numerical studies. Further simplifying assumptions include incompressible flow, constant thermophysical properties of the fluids, and negligible viscous dissipation. The assumption of constant thermophysical properties restricts the applicability of these results to moderate values of temperature difference between the sphere and the bulk.

The governing equations are made dimensionless by using D, U_∞, D/U_∞, ρU_∞^2, $\eta_{ref} = m(U_\infty/D)^{n-1}$, $(U_\infty/D)\eta_{ref}$, and $(U_\infty/D)^2$, respectively, as scaling variables for lengths, velocities,

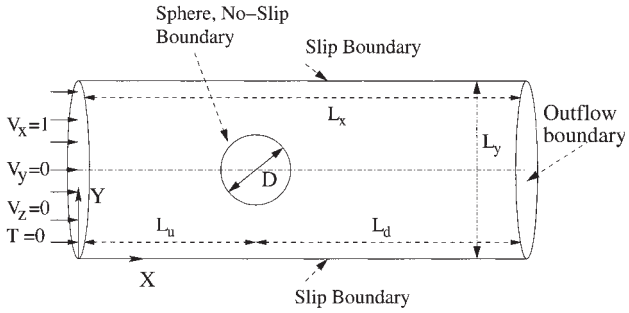

Figure 1. Flow past a sphere.

time, pressure, viscosity, shear stress, and the second invariant of the rate of deformation tensor. The temperature is nondimensionalized as $T' - T_\infty$ divided either by $(T_w - T_\infty)$ or by $(q_w D/k)$, for the CWT and UHF conditions, respectively. All equations and numerical values presented hereafter in this work are in their dimensionless form.

The three-dimensional (3-D) form of the governing equations in the Cartesian coordinates is maintained, given that the source code[29,30] used in the present work is designed to solve 3-D flows in complex geometries, using the Cartesian velocity components and a structured collocated grid. However, symmetry conditions are used in the azimuthal direction as detailed elsewhere[28] so as to simulate only axisymmetric flow conditions.

Continuity Equation

$$\nabla \cdot U = 0 \tag{1}$$

Navier–Stokes Equation

$$\frac{DU}{Dt} = -\nabla p + \frac{1}{\mathrm{Re}} \nabla \cdot \tau_{ij} \qquad \text{where } U = (V_x, V_y, V_z) \tag{2}$$

Energy Equation

$$\frac{DT}{Dt} = \frac{1}{\mathrm{Pe}} \nabla^2 T \tag{3}$$

The rheological equation of state for power law fluids is given by

$$\tau_{ij} = 2\eta \varepsilon_{ij} \tag{4}$$

where $i, j = x, y$ and z and ε_{ij} is the rate of strain tensor, related to the velocity field by

$$\varepsilon_{ij} = \frac{1}{2}\left(\frac{\partial V_i}{\partial j} + \frac{\partial V_j}{\partial i}\right) \tag{5}$$

The viscosity η is given by

$$\eta = (I_2/2)^{(n-1)/2} \tag{6}$$

where n is the power law index ($n < 1$: shear-thinning; $n = 1$: Newtonian liquid; $n > 1$: shear-thickening fluids) and I_2 is the second invariant of the rate of strain tensor whose components are available in standard texts (see Bird et al.[31]).

The dimensionless boundary conditions are given as follows. Given that, in the present work, the momentum equations have been solved by using the pressure–velocity correction method,[30] the boundary conditions for pressure are implemented in terms of a pressure correction, not the true pressure.

- At the inlet boundary

$$V_x = 1 \qquad V_y = 0 \qquad V_z = 0 \qquad \frac{\partial p}{\partial x} = 0 \qquad \text{and} \qquad T = 0$$

- At pipe wall

$$\frac{\partial V_{\tau_t}}{\partial n_t} = 0 \qquad V_{n_t} = 0 \qquad \frac{\partial p}{\partial n_t} = 0 \qquad \text{and} \qquad \frac{\partial T}{\partial n_t} = 0 \qquad \text{(adiabatic)}$$

where n_t and τ_t are the normal and tangential direction to the tube surface, respectively.

- On the sphere surface

$$V_x = V_y = V_z = 0; \qquad \frac{\partial p}{\partial n_s} = 0$$

$$T = 1 \qquad \text{(CWT case)} \qquad \text{or} \qquad \frac{\partial T}{\partial n_s} = -1 \qquad \text{(UHF case)}$$

where n_s represents the unit normal vector on s, the surface of the sphere.

- At the exit boundary. The Orlanski[32] boundary condition has been used at the exit boundary for all dependent variables except for pressure:

$$\frac{\partial \phi}{\partial t} + U_c \frac{\partial \phi}{\partial x} = 0$$

where ϕ is any dependent variable (V_x, V_y, V_z, T) and U_c is the dimensionless average streamwise velocity, which is set equal to 1. The pressure at the outlet is set to a constant value, that is, $p = p_\infty = 0$.

- At the plane of symmetry, that is, at the axis of pipe

$$\frac{\partial V_l}{\partial n_r} = 0 \qquad V_{n_r} = 0 \qquad \frac{\partial p}{\partial n_r} = 0 \qquad \text{and} \qquad \frac{\partial T}{\partial n_r} = 0 \qquad \text{(adiabatic)}$$

where n_r and l are the radial and longitudinal directions, respectively.

The numerical solution of Eqs. 1–3 along with these bound-

ary conditions yields the velocity, pressure, and temperature fields. The resulting temperature field is then used to obtain the local and average Nusselt number, as discussed below.

- The local Nusselt number on the surface of the sphere is evaluated by the following expressions:

$$\mathrm{Nu}_\theta = -\frac{\partial T}{\partial n_s} \qquad \text{(CWT case)} \qquad \text{and}$$

$$\mathrm{Nu}_\theta = -\frac{1}{T}\bigg|_{\text{at sphere surface}} \qquad \text{(UHF case)} \tag{7}$$

These local values have been further averaged over the whole sphere to obtain the surface average (or overall mean) Nusselt number:

$$\mathrm{Nu} = \frac{1}{2}\int_0^\pi \mathrm{Nu}_\theta \sin\theta d\theta \tag{8}$$

The average Nusselt number can be used in process engineering design calculations to estimate the rate of heat transfer from the sphere in the constant wall temperature case, or to estimate the average surface temperature of the sphere for the uniform heat flux condition.

Numerical Methodology

The finite volume method of Eswaran and Prakash[29] for complex 3-D geometries implemented on a nonstaggered (collocated) grid has been used to discretize and solve the governing equations with a semi-implicit scheme with false-transient time-stepping. Thus, all dependent variables V_x, V_y, V_z, T, and p are defined at the centroid of the control volume. The convective terms are discretized using the QUICK scheme,[30,33] whereas the diffusive and non-Newtonian terms are discretized using the central difference scheme. The discretized equations are solved using a Gauss–Seidel iterative algorithm. The simulations are time-stepped from arbitrary initial conditions until steady state is reached. The fully converged steady velocity field obtained from the momentum equations is then used as an input to the energy equation to obtain the steady-state temperature field. Because detailed descriptions of such steps as the solution procedure, choice of numerical parameters, benchmarking for Newtonian, and power law fluid flow and heat transfer from sphere to Newtonian fluids are available elsewhere,[7,28] they are not repeated here.

Results and Discussion

Domain and grid independence

Because the flow studied is an unconfined flow, a finite computational domain is an artificial imposition that should be chosen so that it does not unduly influence the results. The accuracy of the numerical results is contingent on a prudent choice of the domain size and the grid size.

The domain size is defined by three parameters, namely, upstream distance (L_u), downstream distance (L_d), and radius of the pipe ($L_y/2$), as shown in Figure 1. It is important to take a sufficiently large domain so as to simulate the flow over an unconfined sphere. The extensive studies on domain independence carried out previously[7,28] revealed the domain sizes of $130R_s$ and $90R_s$ (that is, $L_u = L_d = L_y/2 = 130R_s$ and $90R_s$) to be sufficient for the Re < 20 and Re > 20 regimes, respectively. The effect of domain size on heat transfer in the power law fluids ($n = 0.6$ and $n = 2$) at Re $= 10$ and Re $= 100$ is presented in Table 1 for two values of Prandtl number. It can be seen from Table 1 that the variation in Nusselt number for different domain sizes is generally within 1%. Similarly, a typical comparison of the local Nusselt number along the sphere surface for different domain sizes for different values of the Reynolds number, Prandtl number, and power law index is shown in Figure 2, where the results are seen to be essentially domain independent. Therefore, based on the comparisons shown in Table 1 and Figure 2, domain sizes of $130R_s$ and $90R_s$ for Re < 20 and Re > 20 regimes, respectively, are regarded to be adequate.

Table 1. Domain Independence Study

Domain Size	Nu at Pr = 5	Nu at Pr = 200
	Re = 10, n = 0.6	
130	5.8313	16.1430
150	5.8889	16.1205
	Re = 10, n = 2	
130	4.7720	13.0002
150	4.7760	13.1004
	Nu at Pr = 5	**Nu at Pr = 20**
	Re = 100, n = 0.6	
90	14.6517	23.2172
150	14.4318	23.2606
	Re = 100, n = 2	
90	10.2496	15.6641
150	10.2483	15.7616

Because a detailed description of the grid used in the present study is available elsewhere,[7,28] only the salient features are recapitulated here. In brief, it consists of the meshing of $0.01D$ near the sphere having 100 control volumes along the half-sphere surface. Although the boundary layer thickness changes with the power law index (n), the grid used in the present work is fine enough to resolve the boundary layer effects[34] for the entire range of parameters used. The grid used in the present work is much finer than that used in other previous studies (see, for example, Tripathi et al.,[35] Tripathi and Chhabra,[36] and Graham and Jones[37]). However, the degree of nonlinearity of the system of equations increases as the value of the power law index deviates increasingly from unity. This makes convergence for the momentum equations difficult for $n \leq 0.6$, as also noted by others.[37-39] Therefore, for n values of 0.5 and 0.6, a somewhat coarser grid was used (radial meshing of $0.03D$ with 60 control volumes around half-sphere for Re > 20 and meshing of $0.05D$ with 60 control volumes around the half-sphere for Re < 20). However, even this coarser mesh was sufficiently fine to resolve the flow inside the boundary layer.

Validation

Drag Coefficient. The solver used in the present study has already been validated extensively for Newtonian fluids[28] and for power law fluids.[7] The maximum difference between the

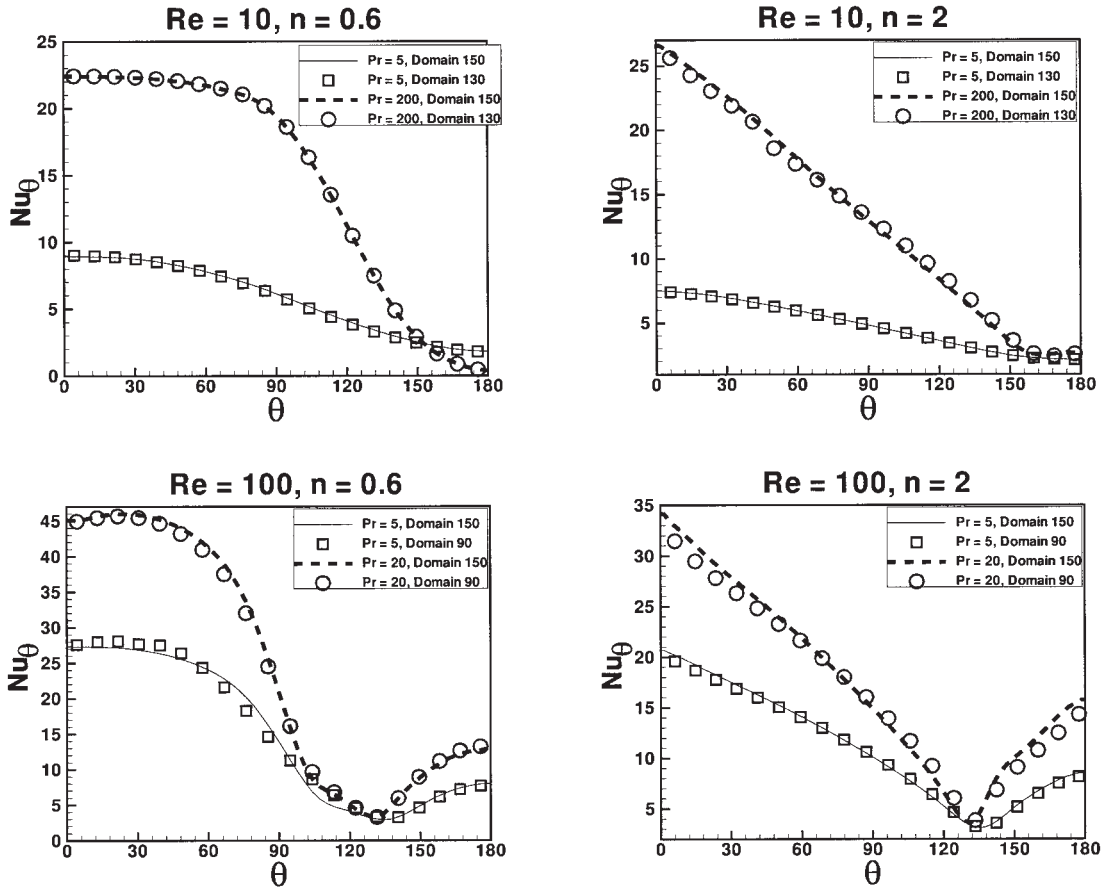

Figure 2. Local Nusselt number variation on the sphere surface for CWT condition at different domain sizes.

present drag values for power law liquids from that of the available numerical studies and experimental studies in the literature was found to be around 3 and 10%, respectively. The possible reasons for these deviations have also been discussed and justified elsewhere.[7]

Nusselt Number. The accuracy and the reliability studies of the energy equation solver used in the present study were carried out extensively for the Newtonian case in our previous study.[28] However, no prior results are available on the forced convection heat transfer from power law fluids to spheres. Because there is no additional term in the energy equation arising from the power law behavior of the fluid, it is reasonable to assume that the accuracy of the heat transfer results for power law fluids will be similar to the accuracy obtained for Newtonian fluids.[28]

Heat-transfer results

Local Nusselt Number. Because of the inherent differences, results for the two thermal boundary conditions used in the present work are discussed separately.

Constant-Temperature Condition (Isothermal Sphere). The variation of the local Nusselt number on the sphere surface for Re values of 5, 50, and 200 for a range of values of the Prandtl number and power law index n is shown in Figure 3. The average Nusselt number increases with an increase in the Reynolds number and/or Prandtl number and/or with decreasing values of n. As n decreases, the liquid becomes more shear-thinning, that is, the effective viscosity of the liquid near the sphere decreases with the increasing Reynolds number and the decreasing value of n. This decrease in viscosity gives rise to larger velocity gradients near the sphere, thereby facilitating convective heat transfer resulting in enhancement of the average Nusselt number. The detailed flow structure around the sphere for different values of n at different Reynolds numbers also supports the idea of enhanced mobility of the fluid near the sphere.[7]

Figures 3a–3i show the relatively large values of the Nusselt number at the front stagnation point ($\theta = 0°$), which decreases gradually along the surface of the sphere, to a minimum value at the rear stagnation point. For Re > 20, that is, when flow separation occurs, Figures 3d–3i show that the Nusselt number decreases from its maximum value at the front stagnation point ($\theta = 0°$) to a minimum value near the point of separation, beyond which a gradual increase in the values of the local Nusselt number can be seen up to the rear stagnation point. The change in the slope in the Nusselt number variation after the separation point is evidently attributed to the existence of a vortex. Furthermore, it is also seen that the local Nusselt number is nearly constant up to about $\theta = 60°$ from the front stagnation point for an n value of 0.5, whereas it starts decreasing right from the front stagnation point for n values of 1 and 2. This seems to suggest poor circulation of the fluid over this part of the sphere surface in the latter case.

The value of the local Nusselt number is also seen to be

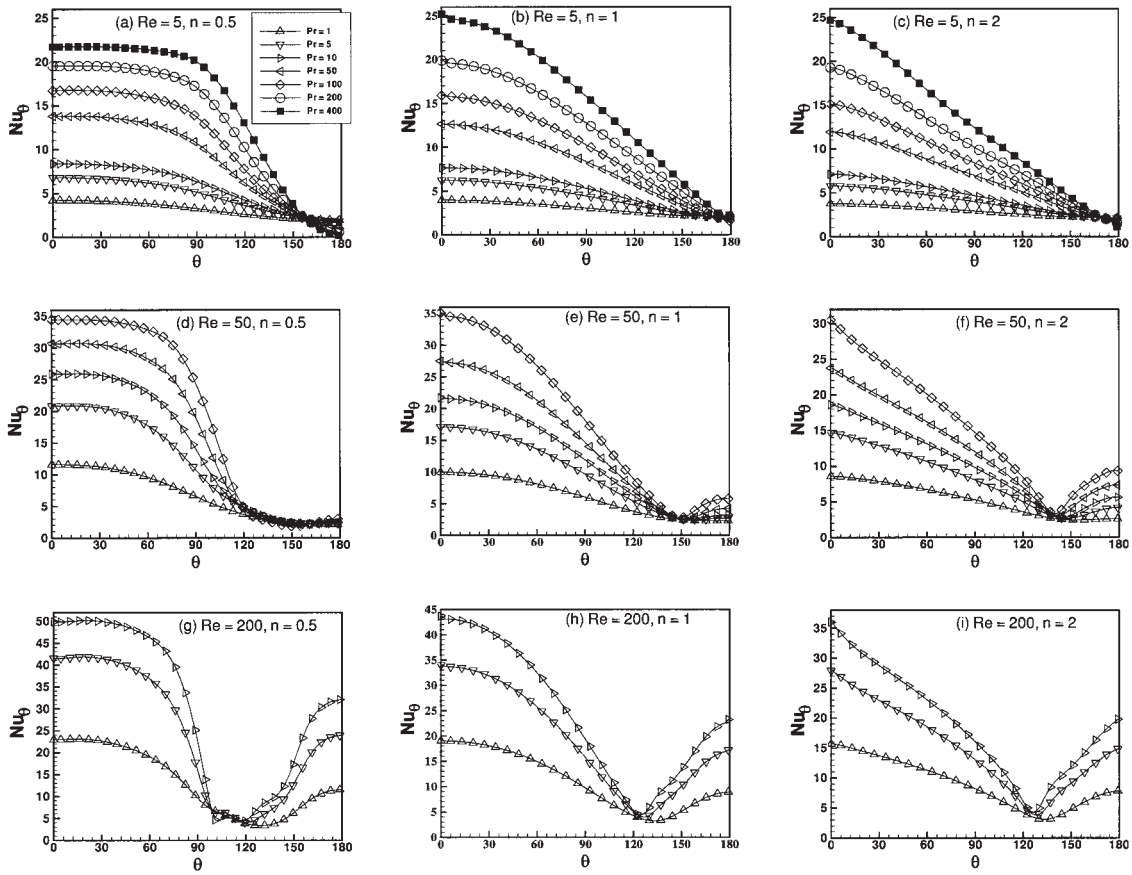

Figure 3. Local Nusselt number variation on the sphere surface for CWT condition.

strongly influenced by the value of the Prandtl number and power law index. At Re = 5 and $n = 0.5$, the local Nusselt number at the front stagnation point increases from 4.20 to 21.72 as the Prandtl number increases from 1 to 400, whereas the change in the Nusselt number at the rear stagnation point is from 1.93 to 0.19, by an order of magnitude. The corresponding figures at $n = 2$ are 3.74 to 24.71 at the front stagnation and 2.12 to 1.12 at the rear stagnation points, respectively. On the other hand, at Re = 200 and $n = 0.5$, the front stagnation point Nusselt number increases from 22.97 to 49.89, whereas the rear stagnation Nusselt number increases from 11.54 to 32 as the Prandtl number increases from 1 to 10, whereas the corresponding figures at $n = 2$ are 15.68 to 36.03 at the front stagnation and 7.82 to 19.78 at the rear stagnation points, respectively. At low Reynolds numbers and Prandtl numbers, there is hardly any variation in the value of the local Nusselt number over the surface of the sphere; this is obviously a consequence of the relatively poor convection. Furthermore, the front stagnation point Nusselt number for Re = 5 and $n = 0.5$ at Pr = 400 is lower than that at Re = 5 and $n = 1$.

Although the exact reasons for this slightly anomalous trend are not immediately obvious, it could be explained by the use of the slightly coarse mesh for $n = 0.5$, as discussed earlier. This effect becomes accentuated, especially at the stagnation points, as a result of the occurrence of steep gradients and boundary layer thickness being zero at this point. Therefore it is likely that the grid used for this condition (Re = 5, $n = 0.5$, and Pr = 400) is not fine enough to capture very high thermal gradients near the front stagnation point giving rise to such a behavior. Although no more explanation can be offered at this stage, suffice it to say here that this anomaly appears to have virtually no influence on the surface-averaged values of the Nusselt number.

Uniform Heat Flux Condition (Isoflux Sphere). Representative results on the variation of Nusselt number on the surface of the sphere for this case are shown in Figures 4a–4i. These figures show qualitatively similar features to those in Figures 3a–3i for the CWT boundary condition and therefore are not discussed in detail.

Average Nusselt Number. The functional relationship between the Nusselt number (Nu), Prandtl number (Pr), power law index (n), and the Reynolds number (Re) is seen to be qualitatively similar for both thermal boundary conditions. Figure 5 shows the effect of n on the average Nu number at different Re numbers and Pr numbers: for the CWT condition at Re = 5 and Pr = 1, the deviation of Nu at $n = 0.5$ and $n = 2$ is 5 and 4%, respectively, from that of Nu at $n = 1$. Respective figures at Pr = 200 are 16% for both cases. Similar deviations at Re = 200 and Pr = 10 are 25 and 22% at $n = 0.5$ and $n = 2$, respectively. So, it can be summarized that the effect of n is significant at high Peclet numbers (Pe = Re × Pr). It is seen that the average Nu number for the sphere increases with the increasing Re number and/or Pr number and/or the decreasing value of n. It should be mentioned here that the slight deviation of the Nu number from the smooth curve at $n = 0.8$ and Re = 200 in Figure 5 is again possibly a result of

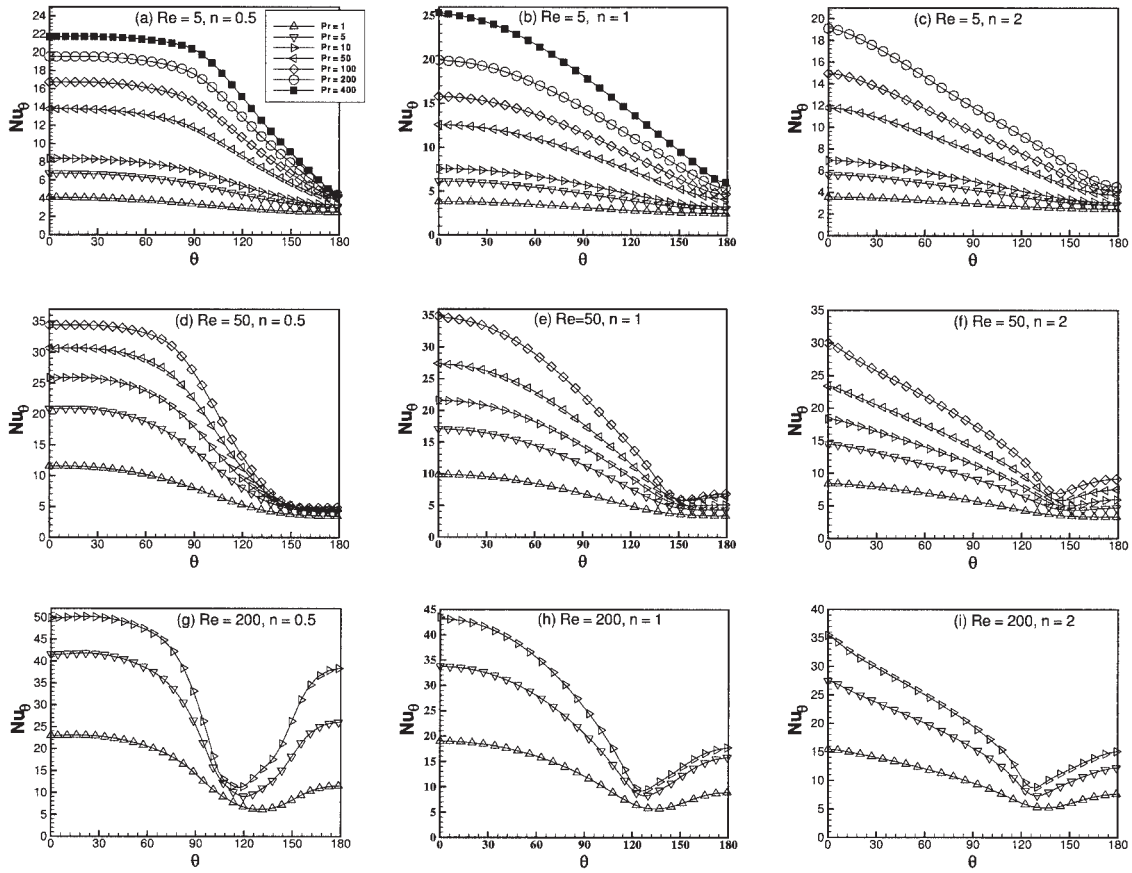

Figure 4. Local Nusselt number variation on the sphere surface for UHF condition.

the different grids used for $n \leq 0.6$ and $n \geq 0.8$ conditions. For the CWT condition, the present numerical data are best fitted by Eq. 9. This equation is based on 278 individual data points embracing wide ranges of conditions ($0.5 \leq n \leq 2$; $1 \leq \mathrm{Pr} \leq 400$; $5 \leq \mathrm{Re} \leq 200$) and it correlates the present numerical data with the maximum and average deviations of 10.2 and 2.6%, respectively. For the Newtonian case (that is, at $n = 1$) it reduces to the correlation proposed by Feng and Michaelides[40] and also at $\mathrm{Re} = 0$ for Newtonian fluids it reduces to the expression of Acrivos.[41] Similarly, Eq. 10 fits the present numerical data (278 data points) for the UHF condition with maximum and average deviations of 10.6 and 2.8%, respectively. At $n = 1$, Eq. 10 reduces to a correlation proposed in our previous study[28] for the UHF condition for Newtonian fluids.

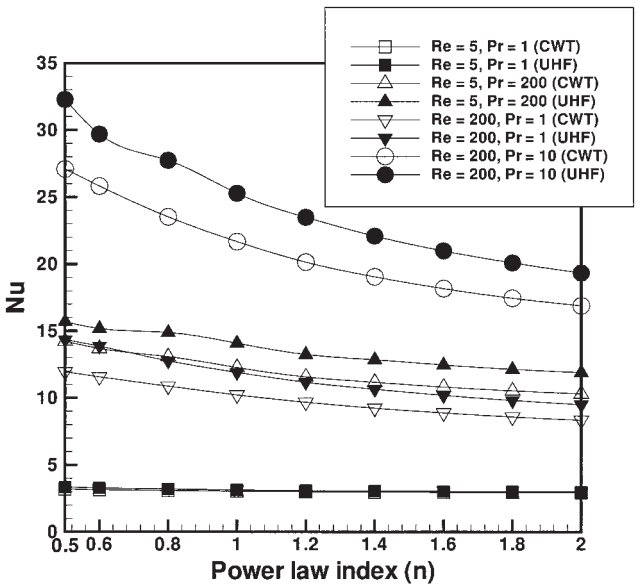

Figure 5. Variation of average Nusselt number with power law index (*n*).

$$\mathrm{Nu} = (0.922 + \mathrm{Re}^{1/(n+2)}\mathrm{Pr}^{1/3} + 0.1\,\mathrm{Re}^{2/3}\mathrm{Pr}^{1/3}) \qquad (9)$$

$$\mathrm{Nu} = (1 + \mathrm{Re}^{1/(n+2)}\mathrm{Pr}^{1/3} + 0.158\,\mathrm{Re}^{2/3}\mathrm{Pr}^{1/3}) \qquad (10)$$

The average Nusselt number is always slightly higher for the UHF condition than that for the CWT condition under otherwise identical conditions, as is indicated by the constants in Eqs. 9 and 10.

Finally, a correlation is also proposed to predict the Nusselt number at the front stagnation point of a sphere. The form of the correlation is maintained identical to that of Eq. 9, only the constant in the last term becomes 0.44 instead of 0.1.

$$\mathrm{Nu}_0 = (0.922 + \mathrm{Re}^{1/(n+2)}\mathrm{Pr}^{1/3} + 0.44\,\mathrm{Re}^{2/3}\mathrm{Pr}^{1/3}) \qquad (11)$$

Equation 11 is applicable for both conditions—CWT and UHF—also indicating that the Nusselt number at the front stagnation point is almost similar for both thermal boundary conditions (as can also be seen from Figures 3 and 4). Equation 11 entails an average deviation of 5.3%. If the data points for extreme cases (that is, Re = 200 and $n = 2$) are excluded, the average deviation drops to 4%. The local Nusselt number data at the rear stagnation point could not be fitted because of the complex flow and temperature fields at the rear stagnation point arising from the wake formation.

Comparison with experimental results

The numerical results obtained using the present scheme for Newtonian liquids ($n = 1$) have been compared with the well-known equation of Whitaker[42] and with the numerical predictions of Feng and Michaelides[40] previously[28] and were found to be within the confidence limits of both these studies.

A similar comparison is attempted here for power law fluids. As mentioned earlier, there are no data available on heat transfer from spheres to power law fluids except for the limited results of Yamanaka and Mitsuishi,[43] who studied mixed-convection heat transfer in power law fluids. Unfortunately, the minimum value of the Prandtl number in their study is about 5×10^4 and they presented an empirical correlation of the form, $\mathrm{Nu} = f(\mathrm{Pe}, \mathrm{Pr}, \mathrm{Gr})$, which reproduced their data with an average error of 30%, which rose to a maximum of 68%. Clearly, it is not possible to make a comparison with their correlation. On the other hand, Ghosh et al.[22] studied mass transfer from benzoic acid spheres suspended in streaming power law fluids. Based on their own and the scant literature data, Ghosh et al.[22] proposed the following correlation for Sherwood number:

$$\mathrm{Sh} = 2 + 0.997\,\mathrm{Re}^{1/2}\mathrm{Sc}^{1/3}\left(\frac{\eta_s}{\eta_b}\right)^{-1/(3n+1)} \qquad (12)$$

where η_s and η_b are the values of the effective viscosity at the surface of the sphere and that in the bulk, respectively. Equation 12 was stated to be applicable over the following ranges of conditions: $n = 0.773$ and $n = 0.854$, $9.5 \times 10^3 \le \mathrm{Sc} \le 1.9 \times 10^6$, and $4 \le \mathrm{Re} \le 200$. They reported the average error to be 12%, though the experimental results deviate by up to roughly 70–80% from Eq. 12. Finally, by invoking the usual analogy between heat and mass transfer, Ghosh et al.[22] also asserted Eq. 12 to be applicable to heat transfer by simply substituting the Nusselt number for the Sherwood number and the Prandtl number for the Schmidt number. Although this analogy seems to have worked well in Newtonian fluids, its extension to power law fluids is less obvious. This approach implicitly assumes that the concentration and temperature dependencies of the effective viscosity are similar and that the term $(\eta_s/\eta_b)^{-1/(3n+1)}$ adequately accounts for this effect. Notwithstanding these factors, coupled with the fact that the minimum value of the Schmidt (Prandtl) number associated with Eq. 12 is much larger than that in the present study, the comparison between the present results and the predictions of Eq. 12 for $0.5 \le n \le 0.8$ shown in Figure 6 must be treated as being qualitative rather than quantitative. The experimental results are always seen to be underpredicted by up to roughly 30%.

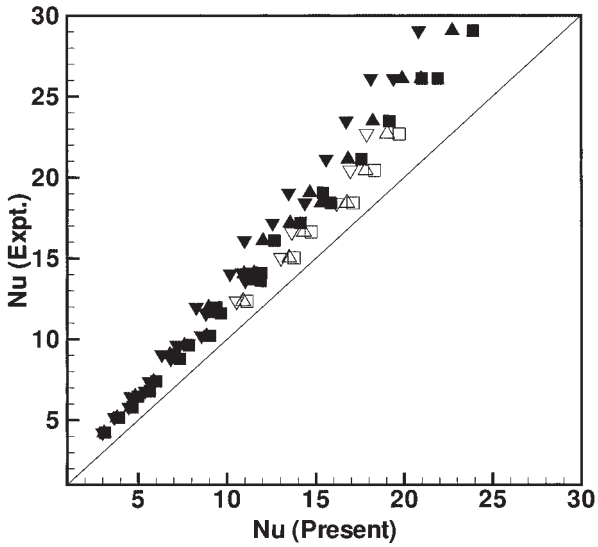

Figure 6. Comparison of the present results with the experimental values for CWT condition.

(Symbols: open symbols for Pr > 50, filled symbols for Pr ≤ 50, □ → n = 0.5, Δ → n = 0.6, ∇ → n = 0.8).

Furthermore, the lower the value of the Prandtl (Schmidt) number, the greater is the deviation. This is hardly surprising in view of the fact that the lowest value of the Schmidt number in Eq. 12 is 9.5×10^4. On the other hand, as the value of n decreases, the correspondence between the two values improves slightly. This is also surprising (and is probably fortuitous), given that Eq. 12 is based on data for two values of n of 0.773 and 0.854.

Finally, although the present simulations relate to an unconfined sphere, experiments always entail wall effects, however small. Depending on the value of the sphere-to-tube diameter ratio, wall effects can give rise to higher velocity (and temperature) gradients that augment the value of the Nusselt number. For instance, the experimental results of Ghosh et al.[22] show this effect to account for up to 20–30% variation in the value of the mass (or heat) transfer coefficient when the sphere-to-tube diameter ratio is of the order of 0.25–0.375, especially resulting from the parabolic velocity profile of the liquid in the tube. In principle, one can argue that the poor agreement seen in Figure 6 could be explained by the temperature dependency of power law viscosity, which has been neglected in the present work, but the numerical results of Westerberg and Finlayson[17] show this factor to enhance the value of the Nusselt number by only 8% for Pe = 100 and $\Delta T = 30$ K. Finally, it is also useful to note here that because Ghosh et al.[22] measured the rate of mass transfer by the weight-loss method, the size (and possibly shape) of the benzoic spheres must be continually changing with time in their experiments. Additional complications can also arise from the size and type of supports used to suspend the benzoic acid spheres in the experimental work.

In summary, bearing all these factors, the comparison seen in Figure 6 must be treated as being qualitative only and is regarded to be encouraging. Obviously, more data and simulations are required to develop universally applicable formulae for the prediction of Nusselt number for spheres immersed in power law fluids.

Conclusions

In this work, the effects of the Reynolds number, Prandtl number ($1 \leq Pr \leq 400$), power law index ($0.5 \leq n \leq 2$), and of the two commonly used thermal boundary conditions on the forced convection heat transfer from an unconfined sphere to power law fluids have been investigated in the Reynolds number range of $5 \leq Re \leq 200$ in the 2-D axisymmetric and steady flow regime. The local Nusselt number variation with the angle from the front stagnation point is shown for various values of the Reynolds number, Prandtl number, and power law index. The average Nusselt number increases monotonically with the Reynolds number and/or Prandtl number and/or the decreasing power law index. Furthermore, whereas the value of the Nusselt number is always higher for the UHF boundary condition than that for the CWT condition, the difference between the two values is a function of Re, Pr, and n. Equations 9 and 10 capture well the dependency of Nusselt number on the Reynolds number, Prandtl number, and power law index. A preliminary comparison with the limited experimental results for $n < 1$ appears to be encouraging; however, no such results are available for shear-thickening ($n > 1$) fluids. A simple expression is also proposed to predict the Nusselt number at the front stagnation point. Future work in this field is obviously required to explore the roles of viscous dissipation, temperature-dependent properties, and the wall effects to make more meaningful comparisons with appropriate experimental results. Also, some refinement in the numerics is needed to resolve the extremely thin boundary layers at high Prandtl numbers.

Notation

c_p = specific heat of the fluid, J kg^{-1} K^{-1}
CWT = constant wall temperature
D = diameter of sphere, m
D_m = diffusion coefficient, m^2/s
h = local convective heat-transfer coefficient, W m^{-2} K^{-1}
$\bar{h}$ = average convective heat-transfer coefficient, W m^{-2} K^{-1}
k = thermal conductivity of the fluid, W m^{-1} K^{-1}
k_c = mass-transfer coefficient, m/s
L_u = upstream length from the inlet to the center of sphere
L_d = downstream length from the center of sphere to the outlet
L_x = length of the computational domain [$=L_u + L_d$]
L_y = height of the computational domain
m = power law consistency index [Pas^n]
n = power law index
n_s = direction normal to the sphere surface
Nu = average Nusselt number [$=\bar{h}D/k$]
Nu_0 = local Nusselt number at the front stagnation point of the sphere [$=hD/k$]
Nu_θ = local Nusselt number of the sphere [$=hD/k$]
p = nondimensional pressure [$p'/\rho U_\infty^2$]
p_∞ = nondimensional pressure at the exit
Pe = Peclet number [Re × Pr]
Pr = Prandtl number [$c_p m(U_\infty/D)^{n-1}/k$]
q_w = heat flux at the surface of the sphere, W/m^2
Re = Reynolds number [$=D^n U_\infty^{2-n}\rho/m$]
R_s = sphere radius, m
Sc = Schmidt number [$m(U_\infty/D)^{n-1}/\rho D_m$]
Sh = Sherwood number [$k_c D/D_m$]
t = time [$=t'/(D/U\infty)$]
T = temperature [$=(T' - T_\infty)/(T_w - T_\infty)$ or $(T' - T_\infty)/(q_w D/k)$]
T_∞ = temperature of the fluid at the inlet, K
T_w = constant wall temperature at the surface of the sphere, K
U_c = average streamwise velocity
U_∞ = uniform velocity of the fluid at the inlet, m/s
UHF = uniform heat flux
V_x = component of the velocity in the x-direction [$=V_x'/U_\infty$]
V_y = component of the velocity in the y-direction [$=V_y'/U_\infty$]
V_z = component of the velocity in the z-direction [$=V_z'/U_\infty$]
x = streamwise coordinate [$=x'/D$]
y = transverse coordinate [$=y'/D$]
z = azimuthal coordinate [$=z'/D$]

Greek letters

η = apparent viscosity of the fluid
ϕ = dependent variable in convective boundary condition
θ = streamwise angle, degree
ρ = density of the fluid, kg/m^3
τ = shear stress
ε = rate of strain tensor

Superscript

$'$ = dimensional variable

Subscripts

l = longitudinal direction
r = radial direction

Literature Cited

1. Clift R, Grace JR, Weber ME. *Bubbles, Drops, and Particles*. New York: Academic Press; 1978.
2. Coulson JM, Richardson JF. *Chemical Engineering*. 4th Edition. New York: Pergamon Press; 1990;1.
3. Churchill SW, Usagi R. A general expression for the correlation of rates of transfer and other phenomena. *AIChE J*. 1972;18:1121-1128.
4. Chhabra RP, Richardson JF. *Non-Newtonian Flow in the Process Industries; Fundamental and Engineering Applications*. Oxford, UK: Butterworth-Heinemann; 1999.
5. Chhabra RP. *Bubbles, Drops and Particles in Non-Newtonian Fluids*. 2nd Edition. Boca Raton, FL: CRC Press; 2006.
6. Renaud M, Mauret E, Chhabra RP. Power law fluid flow over a sphere; average shear rate and drag coefficient. *Can J Chem Eng*. 2004;82: 1066-1070.
7. Dhole SD, Chhabra RP, Eswaran V. Flow of power law fluids past a sphere at intermediate Reynolds numbers. *Ind Eng Chem Res*. 2006; 45:4773-4781.
8. Acrivos A, Shah MJ, Petersen EE. Momentum and heat transfer in laminar boundary layer flows of non-Newtonian fluids past external surfaces. *AIChE J*. 1960;6:312-317.
9. Bizzell GD, Slattery JC. Non-Newtonian boundary layer flow. *Chem Eng Sci*. 1962;17:777-782.
10. Lin FN, Chern SY. Laminar boundary layer flow of non-Newtonian fluids. *Int J Heat Mass Transfer*. 1979;22:1323-1329.
11. Nakayama A. Integral methods for forced convection heat transfer in power law non-Newtonian fluids. In: Cheremisinoff NP, ed. *Encyclopedia of Fluid Mechanics*. Houston, TX: Gulf Publishers; 1988;7:305-339.
12. Nakayama A, Shenoy AV, Koyama H. An analysis for forced convection heat transfer from external surfaces to non-Newtonian fluids. *Warme Stoffubertrag*. 1986;20:219-227.
13. Shenoy AV, Nakayama A. Forced convection heat transfer from axisymmetric bodies to non-Newtonian fluids. *Can J Chem Eng*. 1986;64:680-686.
14. Nakayama A, Shenoy AV, Koyama H. An analysis for friction and heat transfer characteristics of power law non-Newtonian fluid flows past bodies of arbitrary geometrical configuration. *Warme Stoffubertrag*. 1988;22;29-36.
15. Kim HW, Jeng DR, DeWitt KJ. Momentum and heat transfer in power law fluid flow over two dimensional or axisymmetrical bodies. *Int J Heat Mass Transfer*. 1983;26;245-259.
16. Kawase Y, Ulbrecht J. Newtonian fluid sphere with rigid or mobile interface in a shear-thinning liquid; drag and mass transfer. *Chem Eng Commun*. 1981;8:213-231.
17. Westerberg KW, Finlayson BA. Heat transfer to spheres from a polymer melt. *Numer Heat Transfer A*. 1990;17:329-348.
18. Sharma OP, Bhatnagar RK. Low Reynolds number heat transfer from

a sphere in a laminar flow of non-Newtonian fluids. *Z Agnew Math Mech.* 1975;55;235-242.
19. Kawase Y, Mashelkar RA, Ulbrecht J. Particle liquid mass transfer in viscoelastic media. *Int J Multiphase Flow*. 1982;8;433-438.
20. Kawase Y, Ulbrecht J. Mass transfer from spheres submerged in Newtonian and non-Newtonian fluids. *Electrochim Acta.* 1983;28;643-650.
21. Kawase Y, Ulbrecht J. Non-Newtonian fluid-particle mass transfer in granular beds. *AIChE J.* 1983;29;689-691.
22. Ghosh UK, Kumar S, Upadhyay SN. Mass transfer from spherical and nonspherical particles to non-Newtonian fluids. *Polym-Plast Technol Eng.* 1992;31;271-290.
23. Chhabra RP. Heat and mass transfer in rheologically complex systems. In: Siginer DA, DeKee D, Chhabra RP, eds. *Advances in the Rheology and Flow of Non-Newtonian Fluids*. Amsterdam: Elsevier; 1999:Chapter 39.
24. Kumar S, Tripahti PK, Upadhyay SN. On the mass transfer in non-Newtonian fluids. I. Transfer from spheres to power law fluids. *Lett Heat Mass Transfer.* 1980;7;43-53.
25. Ogawa K, Kudora C, Inoue I. Forced convective mass transfer in viscoelastic fluid around a sphere and a cylinder. *J Chem Eng Jpn.* 1984;17;654-656.
26. Hyde MA, Donatelli AA. Mass transfer from a solid sphere to power law fluids in creeping flow. *Ind Eng Chem Fundam.* 1983;22;500-502.
27. Johnson TA, Patel VC. Flow past a sphere up to Reynolds number of 300. *J Fluid Mech.* 1999;378;19-70.
28. Dhole SD, Chhabra RP, Eswaran V. A numerical study on the forced convection heat transfer from an isothermal and isoflux sphere in the steady-symmetric flow regime. *Int J Heat Mass Transfer.* 2006;49;984-994.
29. Eswaran V, Prakash S. A finite volume method for Navier–Stokes equations. Proceedings of the Third Asian CFD Conference, Bangalore, India; 1998:127-136.
30. Sharma A, Eswaran V. A finite volume method. In: Muralidhar K, Sundararajan T, eds. *Computational Fluid Flow and Heat Transfer*. New Delhi, India: Narosa Publishing House; 2003:445-482.
31. Bird RB, Stewart WE, Lightfoot EN. *Transport Phenomena*. 2nd Edition. New York: Wiley; 2002.
32. Orlanski I. A simple boundary condition for unbounded hyperbolic flows. *J Comp Phys.* 1976;21:251-269.
33. Leonard BP. A stable and accurate convective modeling procedure based on quadratic upstream interpolation. *Comput Methods Appl Mech Eng.* 1979;19:59-98.
34. Feng ZG, Michaelides EE. Drag coefficients of viscous spheres at intermediate and high Reynolds numbers. *Trans ASME J Fluid Eng.* 2001;123:841-849.
35. Tripathi A, Chhabra RP, Sundararajan T. Power-law fluid flow over spheroidal particles. *Ind Eng Chem Res.* 1994;33:403-410.
36. Tripathi A, Chhabra RP. Drag on spheroidal particles in dilatant fluids. *AIChE J.* 1995;41:728-731.
37. Graham DI, Jones TER. Settling and transport of spherical particles in power law fluids at finite Reynolds number. *J Non-Newtonian Fluid Mech.* 1994;54:465-488.
38. D'Alessio SJD, Pascal JP. Steady flow of a power law fluid past a cylinder. *Acta Mech.* 1996;117:87-100.
39. Butcher TA, Irvine TF Jr. Use of the falling ball viscometer to obtain flow curves for inelastic, non-Newtonian fluids. *J Non-Newtonian Fluid Mech.* 1990;36:51-70.
40. Feng ZG, Michaelides EE. A numerical study on the transient heat transfer from a sphere at high Reynolds and Peclet numbers. *Int J Heat Mass Transfer.* 2000;43:219-229.
41. Acrivos A. A note on the heat or mass transfer from a small particle freely suspended in linear shear field. *J Fluid Mech.* 1980;98:299-304.
42. Whitaker S. Forced convection heat transfer correlations for flow in pipes, past flat plates, single cylinders, single spheres and flow in packed beds and tube bundles. *AIChE J.* 1972;18:361-371.
43. Yamanaka A, Mitsuishi N. Experimental study on combined forced and natural convective heat transfer from spheres to power law fluids. *Heat Transfer Jpn Res.* 1977;6:85-91.

Manuscript received Jan. 30, 2006, and revision received July 8, 2006.